Supporting Information

Size Optimization of Fire-Extinguishing Microcapsules Fabricated via Non-Planar Microfluidics and Their Performance Study

Ming Cao,†[a] Xiaoshan Jin,†[a] Meirong Yi,†[ae] Xiaoxiao Chen,[ae] Fangsheng Huang,[b] Zhiqiang Zhu,[bc] Shengyun Ji,[d] Ke Li,[a] Yichuan Dai*[a] and Jianfeng Chen*[ae]

(a. College of Advanced Manufacturing, Nanchang University, Nanchang, 330031, China;

b. Institute of Advanced Technology, University of Science and Technology of China, Hefei, Anhui 230088, China

c. Department of Precision Machinery and Precision Instrumentation, University of Science and Technology of China, Hefei, Anhui 230026, China

d. Department of Biomedical Engineering, Washington University in St. Louis, One Brookings DriveSt. Louis, MO 63130, USA

e. Chongqing Research institute of Nanchang University, Chongqing 402660 China)

†These authors contributed equally to this work

*Corresponding Authors

***E-mail: Jianfeng Chen cjf@ncu.edu.cn**

***E-mail: Yichuan Dai daiyc@ncu.edu.cn**

1. **Supporting Figures**

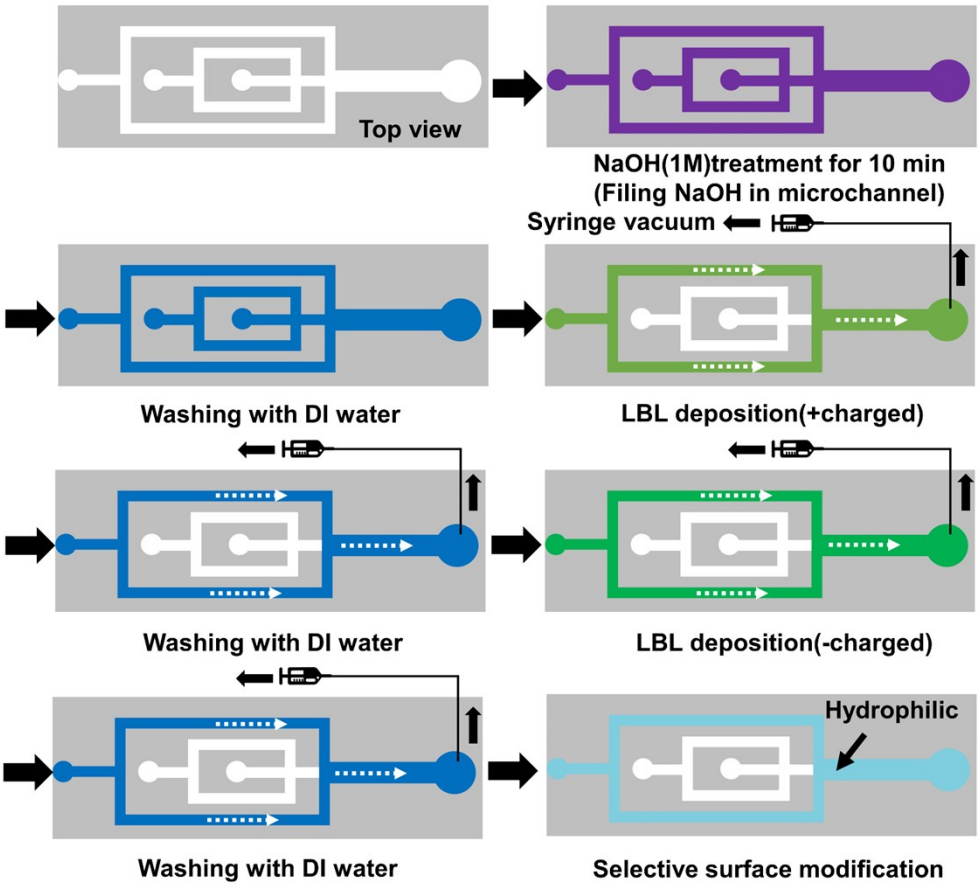

Fig. S1. Schematic diagram illustrating the detailed procedure for spatial patterning of surface wettability on PDMS microfluidic devices (concentrations of both polyelectrolyte solutions: PAH at pH 7.5 and PAA at pH 3.5, were 1 mg/mL).

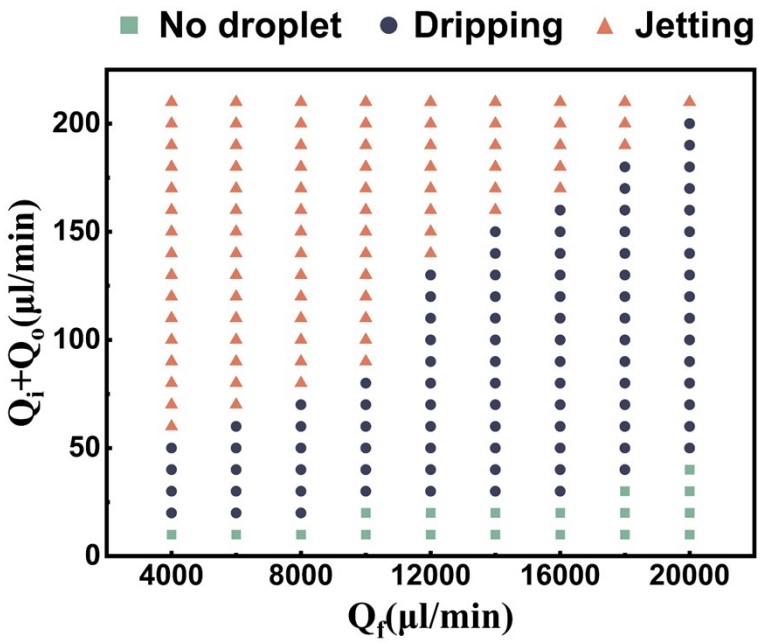

Fig. S2. Flow regime map of microcapsule generation. The operational regions (no droplet, dripping, and jetting) are plotted as a function of the driving phase flow rate (Q_f) versus the combined dispersed phase flow rates (Q_i + Q_o).

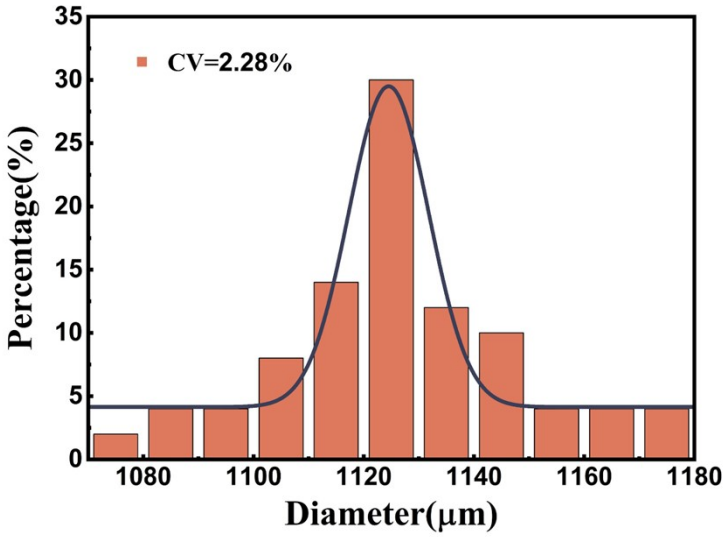

Fig. S3. Size distribution of microcapsules. (Inner phase flow rate Q_i =60μL/min, outer phase flow rate Q_o =60μL/min, driving phase flow rate Q_f =10000μL/min.)

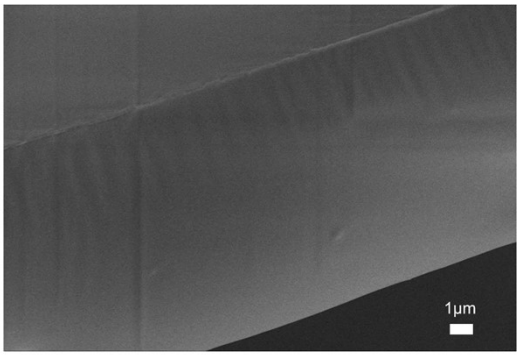

Fig. S4. High-magnification SEM micrograph of the microcapsule shell surface. The image reveals a highly dense, continuous, and smooth topography without any observable micropores, cracks, or pinholes, confirming the structural integrity and hermetic sealing capability of the shell. Scale bar:1μm.

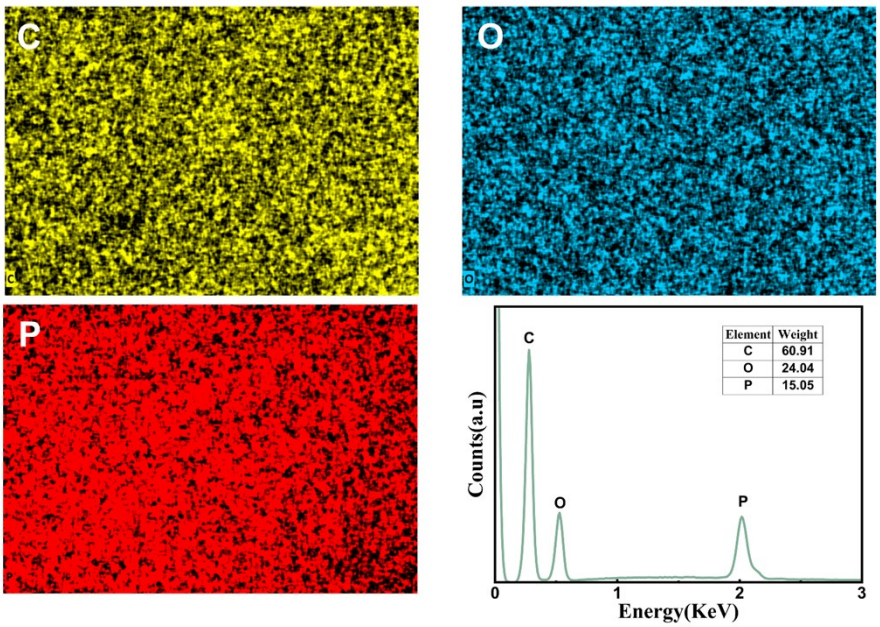

Fig. S5. EDS elemental mapping and corresponding spectrum of the microcapsule shell cross-section. The mapping images display the uniform distribution of Carbon (C), Oxygen (O), and Phosphorus (P) within the resin matrix, while the inset table lists the quantitative elemental weight percentages.

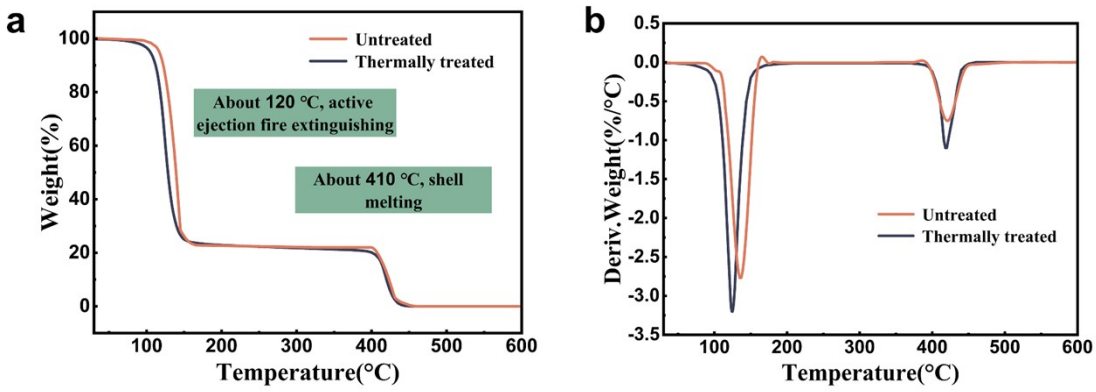

Fig. S6. Comparative thermal stability analysis of untreated and thermally treated microcapsules. (a) TGA and (b) DTG curves exhibiting the weight loss behaviors. The aged samples were subjected to an isothermal treatment at 75 °C for 600 min. The overlapping curves confirm that the accelerated aging process induced negligible loss of the core agent or degradation of the shell material.

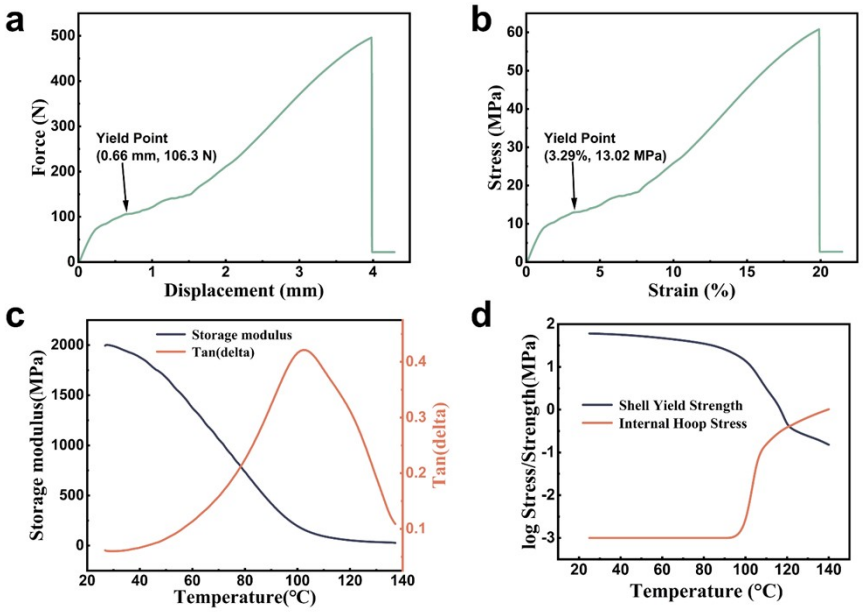

Figure S7. Mechanical characterization of the microcapsule shell material and theoretical rupture analysis. (a) Force-displacement curve and (b) the corresponding stress-strain curve of the cured photoresin film, indicating the mechanical yield point at room temperature. (c) Dynamic Mechanical Analysis (DMA) profiles showing the temperature-dependent evolution of storage modulus and tan delta. (d) Theoretical failure model plotting the calculated internal hoop stress (orange line) against the temperature-dependent yield strength of the shell (blue line). The intersection point at approximately 120 °C corresponds to the predicted rupture onset temperature.

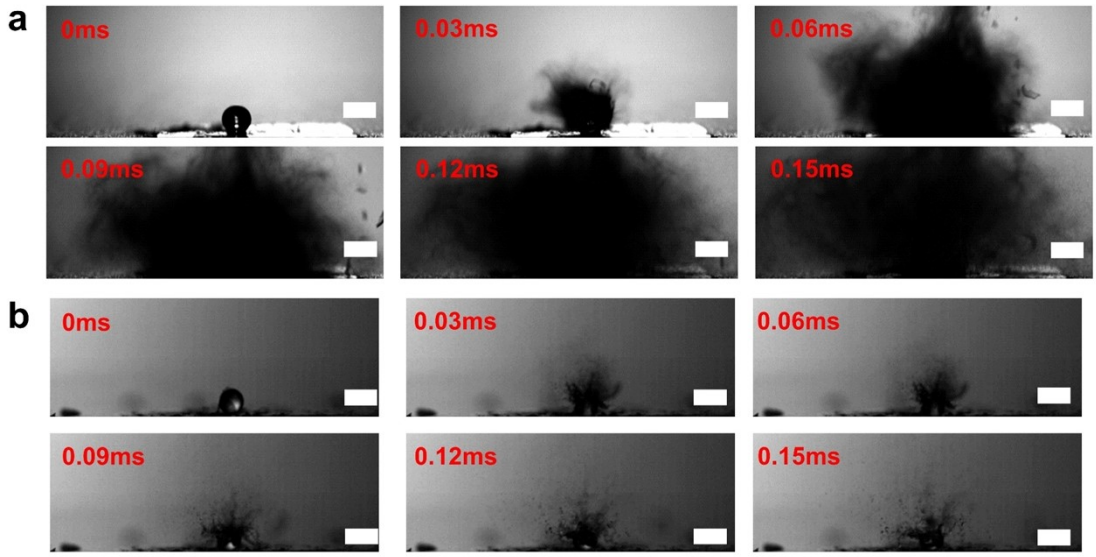

Fig. S8. High-speed camera sequences comparing the thermally triggered rupture behaviors. (a) Microcapsule loaded with 4wt% SDBS, exhibiting a "Flash Atomization Regime" characterized by the rapid expansion of a fine mist cloud. (b) Microcapsule with a pure water core (without surfactant), displaying a "Splashing Regime" with limited expansion and coarse droplet formation. Scale bar: 1 mm.

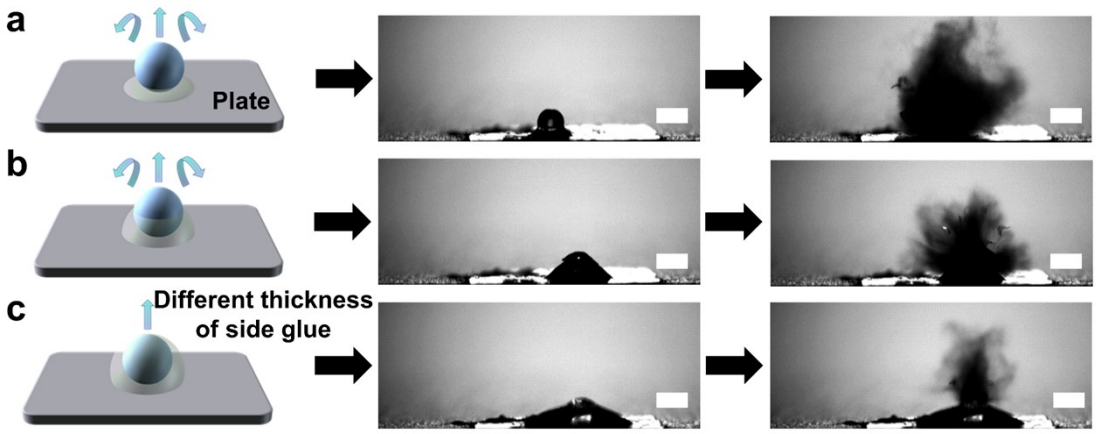

Fig. S9. As shown in (a), (b), and (c), the release range of the microcapsules decreases with increasing adhesive thickness. The spatial release behavior of the microcapsules under different adhesive thicknesses was captured using high-speed photography. Scale bar: 1 mm.

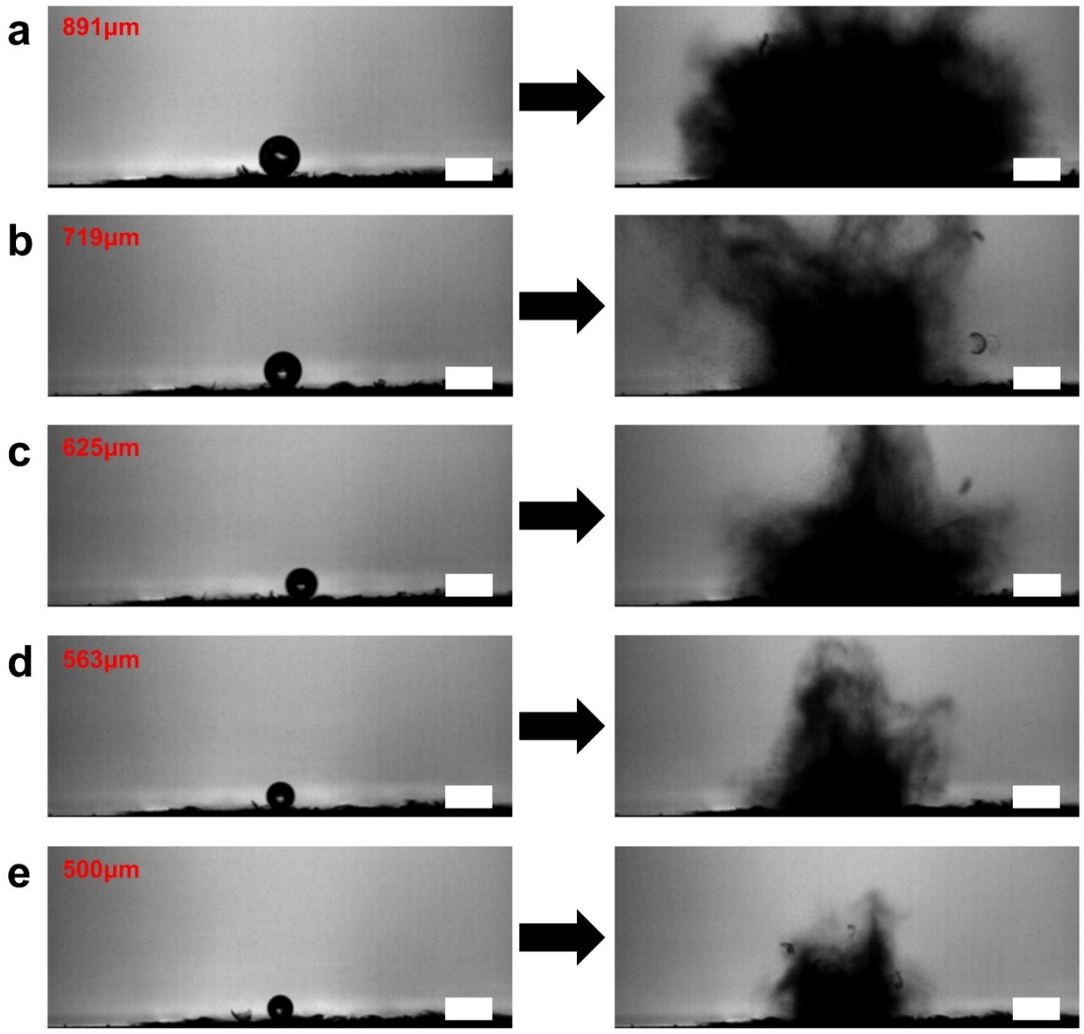

Fig. S10. As shown in (a)–(e), the release range of the water-based microcapsules increases with larger microcapsule diameter. The spatial release behavior of microcapsules with different sizes was captured using high-speed photography. Scale bar: 1 mm.

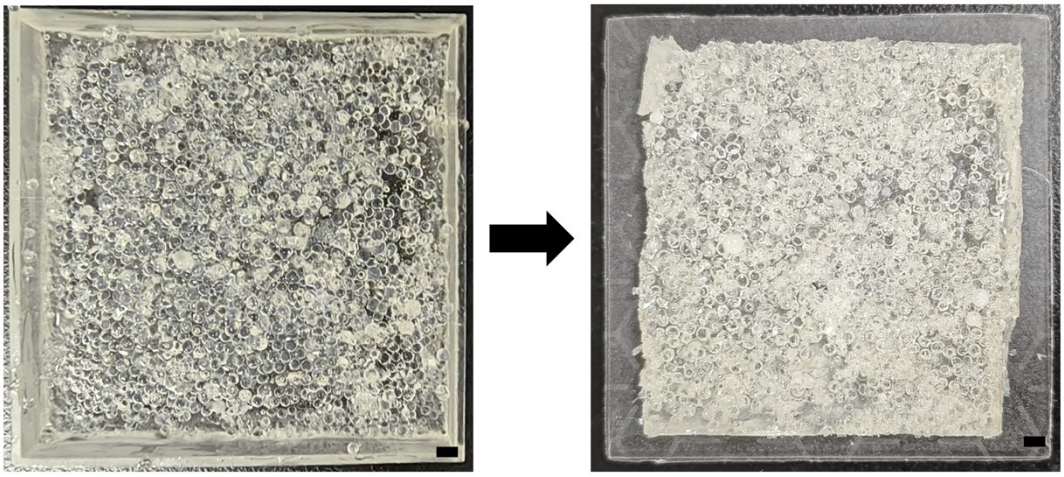

Fig. S11. Photograph of the fire-extinguishing patch. Scale bar: 1 mm.

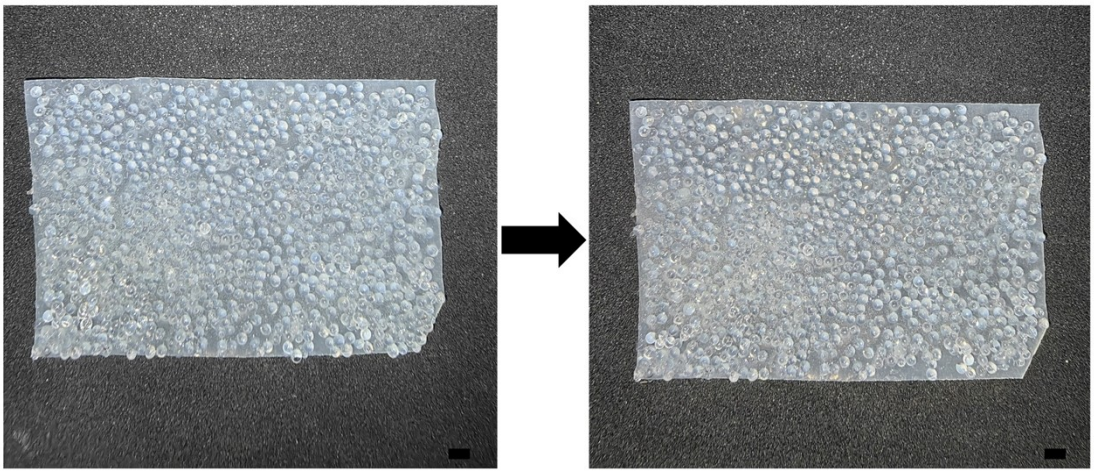

Figure S12. Digital photographs of the fire-extinguishing patch (a) before and (b) after the mechanical vibration test (600 rpm, 60 min). The patch maintained a mass retention of 97.5%. The minor detachment observed at the edges is attributed to the disruption caused by manual cutting (edge effect), while the main functional area remained intact.

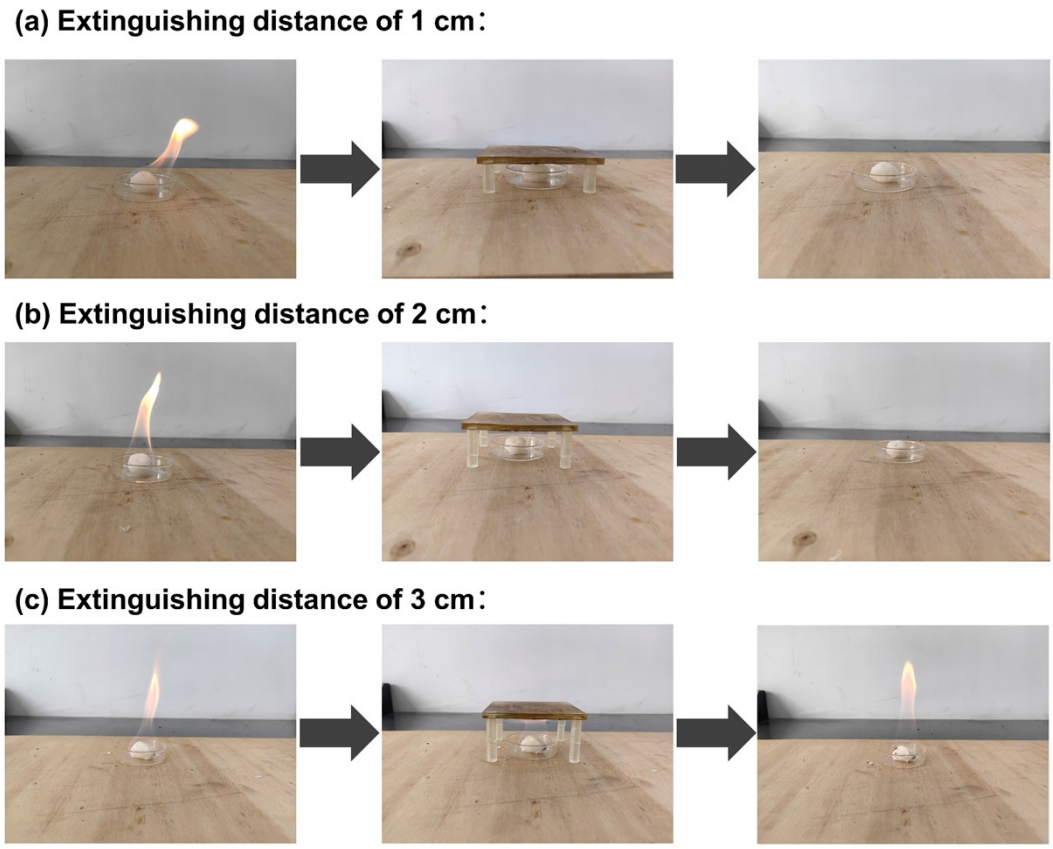

Fig. S13. Fire suppression performance of the microcapsule-based patch at different extinguishing distances: (a) 1 cm. (b) 2 cm. (c) 3 cm.

2. Derivation of the Shell Thickness Formula for Water-Based Microcapsules

2.1. Physical model assumptions

The inner phase (core material) with flow rate Q_i forms the core (a sphere of diameter d_c).

The outer phase (shell precursor) with flow rate Q_o forms the shell (encapsulating the core),with total diameter D .The shell thickness is defined as:

$$d = \frac{D - d_c}{2} \tag{S1}$$

Within the same time period t, the volume of the core is:

$$V_i = Q_i \cdot t \tag{S2}$$

and the volume of the shell is:

$$V_o = Q_o \cdot t \tag{S3}$$

Thus, the ratio of the volumes satisfies:

$$\frac{V_i}{V_o} = \frac{Q_i}{Q_o} \tag{S4}$$

2.2. Combination of geometric relations and volume conservation

The volume of the core is given by:

$$V_i = \frac{4}{3}\pi(\frac{d_c}{2})^3 \tag{S5}$$

The total volume (core + shell) is:

$$V_{total} = \frac{4}{3}\pi(\frac{D}{2})^3 \tag{S6}$$

The volume of the shell is therefore:

$$V_o = V_{total} - V_i = \frac{4}{3}\pi[(\frac{D}{2})^3 - (\frac{d_c}{2})^3] \tag{S7}$$

Combining with the volume ratio derived earlier in Eq S4, and simplifying, yields:

$$(\frac{d_c}{D})^3 = \frac{Q_i}{Q_i + Q_o} \Rightarrow d_c = D \cdot (Q_i / (Q_i + Q_o))^{1/3} \tag{S8}$$

2.3. Derivation of shell thickness formula

Substitute the core diameter d_c from Eq. S8 into the definition of shell thickness given in Equation (S1) yields:

$$d = \frac{D}{2} \cdot [1 - (Q_i / (Q_i + Q_o))^{1/3}] \tag{S9}$$

3. **Supporting Videos**

Movie.S1. Candle Extinguishment Experiment.

Movie.S2. High-Speed Recording of Microcapsule Bursting Process.

Movie.S3. High-Speed Recording of Candle Extinguishment Using Microcapsules.

Movie.S4. Fire Extinguishing Experiment with Thermally Responsive Patch.

4.Supplementary Table

Table S1. Comparison with previous reports on fire-extinguishing microcapsules.

No.	Preparation Method	Shell / Core Materials	Size Distribution	Trigger Temp. (℃)	Long-Term Stability	Loading Tunability	EE (wt%)	Application	Performance	Ref.
1	Interfacial polycondensation	PMMA / DMTP	Polydisperse	95	5% loss after 12 h	Fixed by Formulation	-	Battery separator (PE) + electrolyte	PMMA-coated PE separator: Max. temp. during TR reduced from 72.3 ℃to 56.2℃ ; Microcapsule-coated PE + electrolyte: Max. temp. reduced to 37.2 ℃	[1]
2	Coacervation	Melamine-urea-formaldehyde / Perfluoro(2-methyl-3-pentanone) and heptafluorocyclopentane	Polydisperse	128.9	-	Fixed by Formulation	43.12	Li-ion battery aluminum plastic film	Battery temperature decreased from 800 ℃ to 30℃ within 15 s	[2]
3	Coacervation	Double-layered	Polydisperse	130–140	MC: 14% loss	Fixed by	40	Electrical	Flame extinguished	[3]

	and in situ polymerization	polymer shell (UF resin) / MNFB			after 100 days; DL-MC: 0.005% loss after 100 days	Formulation		fire	naturally after 61 s; Extinguishing times for MC and DL-MC were 36 s and 27 s, respectively	
4	Vacuum impregnation	Hollow mesoporous silica / TEP and PCM (stearic acid)	Relatively Uniform	150	-	Fixed by Formulation	38–45	Battery separator (PP)	PP separator: 33.8% residual weight after 4 s burning; SiO_2-coated: extinguished within 3 s (56.2% residual); PCM-TEP@SiO_2/PP: extinguished within 1 s (84.6% residual)	[4]
5	Coacervation	Crosslinked PMMA (x-PMMA) / TEP	Polydisperse	150–215	-	Fixed by Formulation	-	Battery separator (PE)	Ref pouch: Voltage dropped to 0 V within 8 min; Pouch cell with F-CCS (CE73): Voltage remained stable after 25 min	[5]
6	Microfluidic flow-focusing	Photosensitive resin / Perfluorohexanone	Strictly Monodisperse	110	-	Flow-rate Tunable	75	Electrical sockets	Fire in Type B socket was rapidly extinguished; Fire	[6]

									in Ref socket continued to burn	
7	In situ polymerization	Prepolymer / Perfluorohexanone and 1,1,1,2,2,3,3,4,4-nonafluoro-4-methoxybutane	Polydisperse	-	-	Fixed by Formulation	40	NCM18650 battery surface	Coated 18650 NCM battery: Delayed TR onset by 250 s and even cut off the TRP	[7]
8	In situ polymerization	Melamine, urea, formaldehyde / Hydrates	Polydisperse	100	-	Fixed by Formulation	-	Electrolyte of 1 Ah NCM/Gr 811 pouch cell	Adding only 0.25 g microcapsules increased TR trigger temp. by 16.2 ℃ and reduced max. temp. by 117.5 ℃	[8]
9	Liquid-driven co-flow microfluidics	Flame-retardant photosensitive resin / 3 wt% SDBS aqueous solution	Strictly Monodisperse (CV=2.29%)	130	-	Flow-rate Tunable	26.5, 48, 71.6	Electrical sockets	Fine water mist microcapsules rapidly extinguished flames within 1ms	[9]
10	Low-temperature complex coacervation	Gelatin, sodium polyphosphate (SP) and glutaraldehyde / Perfluorohexanone	Polydisperse	130	4.45% loss after 1 year	Fixed by Formulation	82.27	107 silicone rubber	Surface temperature of silicone rubber decreased from	[10]

									485.9 ℃ to 183.7℃	
11	Coacervation	Gelatin (GE) and Arabic gum (GA) / Perfluorohexanone	Polydisperse	125	6.5% loss after 30 days	Fixed by Formulation	58.6	-	Shortened the self-extinguishing time from 82 s to 35 s	[11]
12	Microfluidics	Photosensitive resin / Perfluorohexanone	-	115–122	-	Flow-rate Tunable	26.7	Various patches	Completely extinguished ignited cotton ball flames within 2 s	[12]
13	In situ polymerization	Polyurea / Perfluorohexanone	Polydisperse	160–220	6.5% loss after 15 days	Fixed by Formulation	69–85	Aerogel sheet	Lowered the temperature rise rate from 41.5℃/s to 30.6℃/s	[13]
14	Non-planar Microfluidics	Photoresin / Water (with SDBS)	Strictly Monodisperse (CV = 2.28%)	120	Accelerated thermal aging tests were conducted to evaluate thermal stability. Microcapsules exhibited only 2.39% negligible	Flow-rate Tunable	85	Various patches	Completely extinguished ignited alcohol cotton flames within 3 s	This Work

					mass loss after continuous exposure at 75 °C for 600 min					

References：

[1] T. Yim, M.-S. Park, S.-G. Woo, H.-K. Kwon, J.-K. Yoo, Y. S. Jung, K. J. Kim, J.-S. Yu and Y.-J. Kim, Nano Letters, 2015, 15, 5059-5067.

[2] W. Zhang, L. Wu, J. Du, J. Tian, Y. Li, Y. Zhao, H. Wu, Y. Zhong, Y.-C. Cao and S. Cheng, Materials Advances, 2021, 2, 4634-4642.

[3] D. H. Lee, S. Kwon, Y. E. Kim, N. Y. Kim and J. B. Joo, Materials, 2022, 15.

[4] Z. F. Liu, Y. T. Peng, T. Meng, L. Yu, S. Wang and X. L. Hu, Energy Storage Materials, 2022, 47, 445-452.

[5] Y. Roh, D. Kim, D. H. Jin, D. Kim, C. L. Han, J. Choi, H. Lee, Y. G. Lee and Y. M. Lee, Chemical Engineering Journal, 2023, 474.

[6] C. Li, H. R. Bian, D. Ding, F. S. Huang and Z. Q. Zhu, Lab on a Chip, 2024, 24, 904-912.

[7] Y. B. Guo, X. J. Wang, J. J. Gao, Z. W. He, S. Yao, X. M. Zhou and H. J. Zhang, Journal of Energy Storage, 2024, 93.

[8] J. J. Tong, Y. Peng, J. Liu, L. Wang, B. W. Hou, X. N. Feng and M. G. Ouyang, Applied Physics Letters, 2024, 125.

[9] Y. J. Ren, P. Zhang, H. R. Bian, D. Ding, C. Li, N. Sang, J. C. Zhang, F. S. Huang and Z. Q. Zhu, Chemical Engineering Journal, 2025, 503.

[10] J. C. Li, Y. D. Xing, H. M. Liu, L. W. Lu, T. Xue, X. Xu and F. Zhang, Composites Communications, 2025, 53.

[11] Z. Y. Han, J. Yang, Y. Yu and X. R. Zhang, Process Safety and Environmental Protection, 2025, 193, 772-780.

[12] Q. S. Pan, N. Sang, T. P. Zhou, C. Z. Wu, T. Si, F. S. Huang and Z. Q. Zhu, Lab on a Chip, 2025, 25, 2193-2204.

[13] Y. Y. Xiao, Y. L. Pan, J. Yang, L. L. Li, Z. Zhao, X. D. Cheng and H. P. Zhang, Chemical Engineering Journal, 2025, 516.